

# RGO@SiC porous films for multilayer electromagnetic shielding

LI Jing\*, Qi Yi-quan, ZHAO Shi-xiang, QIU Han-xun, YANG Jun-he, YANG Guang-zhi\*

(School of Materials and Chemistry, University of Shanghai for Science and Technology, Shanghai 200093, China)

**Abstract:** Developing lightweight and flexible thin films for electromagnetic interference (EMI) shielding is of great significance. In this paper, RGO@SiC porous thin films for EMI shielding were prepared by chemical reduction of mixtures of graphite oxide (GO) and SiC whiskers with HI, followed by microwave irradiation for 3 s. A significant increase of the film thickness from around 20 to 200  $\mu\text{m}$  and further reduction of GO were achieved due to formation of a porous structure via expansion of interlayer space of GO with gases released by heating in 3 s of solid phase microwave irradiation. The total shielding effectiveness ( $SE_T$ ) and the reflective SE ( $SE_R$ ) of the RGO@SiC porous thin films were altered by the GO/SiC mass ratio, which reached the highest  $SE_T$  of 35.6 dB while the  $SE_R$  was only 2.8 dB when the ratio was 12:3. The addition of SiC whiskers was critical for the multi-reflection, interfacial polarization and dielectric attenuation of EM waves. A multilayer composite with a gradient change from transmission to reflection of RGO@SiC porous films was constructed. The highest  $SE_T$  reached 75.1 dB with a  $SE_R$  of 2.7 dB for a film of a thickness of about 1.5 mm when the reflective side of the multilayer composite was stacked on a reflective buckypaper derived from multi-walled carbon nanotubes. We believe that the porous RGO@SiC thin films were promising for designing a multilayer or sandwich structure for EMI absorption in packaging or lining.

**Key words:** Graphene; Thin films; Silicon carbide whiskers; Electromagnetic interference shielding

## 1 Introduction

Carbon-based electromagnetic interference (EMI) shielding materials feature low density, diverse forms and tunable properties. Electrical conductivity of carbon materials has a wide range, depending on their crystal structures, chirality, oxidation degree, etc.<sup>[1,2]</sup> Compared to metal materials, carbon-based materials give the opportunity to construct lightweight, flexible, absorption-dominated EMI shielding materials<sup>[3]</sup>.

Graphene-based thin films can be considered as a two-dimensional (2D) assembly of graphene layers which can be applied as the core layer in sandwich structure, packaging and lining materials for EMI shielding purpose<sup>[4,5]</sup>. Graphene oxide (GO) with a large number of oxygen-containing functional groups can be easily dispersed in water and aligned in thin films by liquid casting, vacuum filtration and electrodeposition. EMI shielding effects can be realized by restoring the electrical conductivity of the thin films upon reduction. However, the high electrical conductivity of reduced GO (RGO) may promote the

reflection of electromagnetic (EM) radiation, resulting in reduction in absorption<sup>[4]</sup> because the reflection of EM radiations is a result of the interactions between the EM waves and free charges of carbon materials<sup>[6]</sup>. Iodine-doped RGO papers with an electrical conductivity of  $10^3$  S/cm showed an EMI shielding effectiveness (SE) of 52.2 dB and SE reflection ( $SE_R$ ) of 18.6 dB<sup>[7]</sup>, which may cause secondary EMI pollution.

RGO-based composite thin films were designed to improve the absorption of EMI. The addition of magnetic and semiconductive materials can promote EM attenuation, such as  $\text{Fe}_3\text{O}_4$ <sup>[8]</sup>,  $\text{MnO}$ <sup>[9]</sup> and  $\text{SiC}$ <sup>[10]</sup>. SiC whiskers/MnO/RGO composites were constructed for improving EMI absorption, where SiC whiskers can dielectrically attenuate EM waves as a semiconductor<sup>[11]</sup>. Synergistic effects on EMI shielding were expected by combining SiC with a conductive phase, such as carbon nanotube-carbon fiber/SiC<sup>[12]</sup> and SiC/MXene/polymer<sup>[13]</sup> composites.

Compared with 2D composite thin films with RGO layers, three-dimensional (3D) assembly of

Received date: 2024-01-31; Revised date: 2024-04-19

Corresponding author: LI Jing, Professor. E-mail: [lijing6080@usst.edu.cn](mailto:lijing6080@usst.edu.cn);

YANG Guang-zhi, Professor. E-mail: [yanggzhi@usst.edu.cn](mailto:yanggzhi@usst.edu.cn)

Homepage: <http://xxtcl.sxice.ac.cn/> CSTR: 32158.14.S1872-5805(24)60855-3

graphene or RGO layers provided graphene monoliths with high porosity and low density. The EMI SE of RGO monoliths mainly came from the direct absorption and the absorption of multiple-reflected EM radiations, which were facilitated by their high porosity and large surface area<sup>[6]</sup>. The EMI SE of RGO monoliths can also be tuned by composite design, such as infiltration of conductive polymers<sup>[6]</sup>, Fe<sub>3</sub>O<sub>4</sub>, carbon nanotubes<sup>[14]</sup> and MXene<sup>[15]</sup>. Porous structure was also reported for MXene/RGO flexible thin film, which had a total SE ( $SE_T$ ) of 55.2 dB with a thickness of only 32  $\mu\text{m}$ , but the high electrical conductivity of  $10^3$  S/cm, resulting in a  $SE_R$  value of around 20 dB<sup>[16]</sup>.

Construction of multilayer composites was another strategy to improve the absorption of EM radiation. The multilayer structure with varying EMI SE of each layer could trap and attenuate the entered EM waves by repeated adsorption, reflection, and scattering in the composite film. The EMI SE of the Fe<sub>3</sub>O<sub>4</sub>@RGO/MWCNT/waterborne polyurethane (WPU) multilayer composites reached 35.9 dB using MWCNT/WPU as the reflection layer<sup>[17]</sup>. The gradients and sequence of the Fe<sub>3</sub>O<sub>4</sub>@RGO layers played an important role on the absorption/reflection ratio. A reflection layer with high electrical conductivity was usually employed to reduce the EM transmission, including Ag/glass fibers<sup>[18]</sup> and MWCNT buckypaper<sup>[19,20]</sup>. EMI SE of over 100 dB was obtained by a sandwich structure of multilayer buckypaper and wave-transmitting layers with a  $SE_R$  of around 15 dB and a thickness of over 20 mm<sup>[20]</sup>.

In this study, RGO@SiC porous thin films were fabricated with the assistance of solid phase microwave irradiation. The amount of SiC whiskers in the RGO@SiC thin films was critical for generating the porous structure and controlling the reduction degree of RGO. The absorption-dominated EMI shielding was realized by the dielectric attenuation of EM waves by SiC, the multi-reflection in the porous thin films and the interfacial polarization between SiC and RGO. In addition, a MWCNT buckypaper was adhered to the RGO@SiC porous film for further im-

proving EMI while remaining the flexibility.

## 2 Experimental

### 2.1 Preparation of RGO@SiC

4 g SiC whiskers (Hebei Chuancheng Metal Materials) was dispersed in 40 mL H<sub>2</sub>O<sub>2</sub> under stirring, followed by washing, filtration and drying. Then, 3-triethoxysilylpropylamine was hydrolyzed at a concentration of 2% when the pH value was adjusted to 4 by acetic acid. 4 g SiC powder reacted with 60 mL silane solution for 24 h at room temperature. The silane-treated SiC was obtained after washing and filtration. GO (5 mg·mL<sup>-1</sup>, Anguqiang Graphene Technology) was mixed with the treated SiC by sonication for 30 min. The mixture was casted in a polytetrafluoroethylene Petri dish and dried in the oven at 60 °C for 24 h to prepare GO@SiC thin films. The GO/SiC weight ratios were 12 : 0, 12 : 1, 12 : 2, 12 : 3 and 12 : 4 for different samples.

The GO@SiC films were reduced firstly by HI (55%–57%) in a hydrothermal autoclave at 90 °C for 1 h. After repeated washing and drying, the thin films were then put into a microwave oven (M1-L213B, output 700 W) for 3 s for secondary reduction to obtain RGO@SiC thin films. The samples were named RGO@SiC0, RGO@SiC1, RGO@SiC2, RGO@SiC3 and RGO@SiC4, according to the SiC content.

### 2.2 Fabrication of RGO@SiC/buckypaper multilayer composites

MWCNTs were dispersed in DI water at a concentration 0.5 mg/mL using 0.5% (mass fraction) of Triton X-100 as the dispersant in an ultrasonic homogenizer (JY96-IIN) for 30 min. The suspension was then filtered using a cellulose filter membrane (0.22  $\mu\text{m}$  pore size) and the buckypaper was obtained after washing and drying. The RGO@SiC thin films were adhered to the buckypaper with WPU (WPU, New City Engineering Plastics) by a glass rod. The fabrication procedure of RGO@SiC/buckypaper multilayer composites was shown in Fig. 1.

### 2.3 Characterization

The morphology of the thin films was investigated by scanning electron microscopy (SEM, FEI

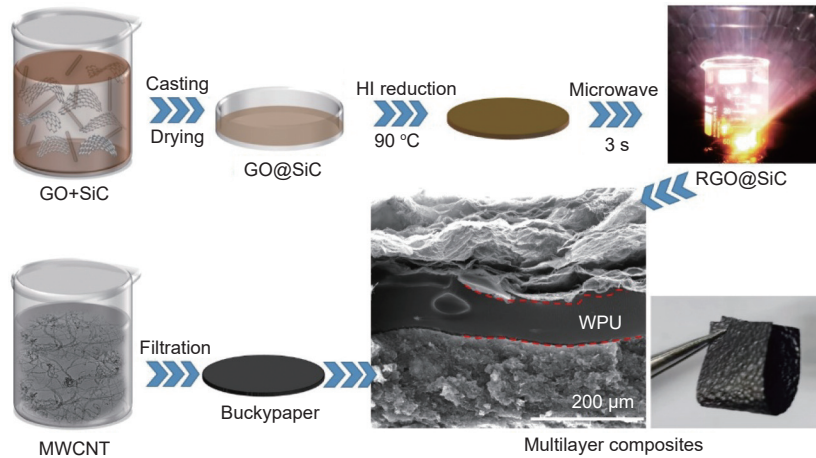


Fig. 1 Fabrication procedure of RGO@SiC/buckypaper multilayer composites

Quanta FEG). X-ray diffraction (XRD, D8 Advance, Bruker), Raman spectrometer (LabRAM, Horiba) and Fourier infrared spectrometer (FTIR, Spectrum 100 PerkinElmer) were employed to characterize the material structure. The thermal stability of the thin films was studied by thermal gravimetric analyzer (TGA, Pyris 1). The specific surface area of the porous thin films was analyzed by the Brunauer-Emmett-Teller (BET) method using ASAP2020. The electrical conductivity and the  $S$  ( $S_{11}$ ,  $S_{21}$ ,  $S_{22}$ ,  $S_{12}$ ) parameters of the thin films were characterized using a four-probe system (RTS-9, MTI Corporation) and a vector network analyzer (Keysight E5063A), respectively. The  $S$  parameters allow the calculation of the total SE ( $SE_T$ ), absorption SE ( $SE_A$ ) and reflection SE ( $SE_R$ ),

according to the Equation 1-6, where the multiple internal reflections ( $SE_M$ ) is negligible if EMI  $SE_T \geq 10$  dB<sup>[6,17]</sup>.

$$R = |S_{11}|^2 = |S_{22}|^2 \quad (1)$$

$$T = |S_{21}|^2 = |S_{12}|^2 \quad (2)$$

$$A = 1 - R - T \quad (3)$$

$$SE_R = -10\lg(1 - R) \quad (4)$$

$$SE_A = -10\lg[T / (1 - R)] \quad (5)$$

$$SE_T = SE_R + SE_A + SE_M \quad (6)$$

## 3 Results and discussion

### 3.1 Structure and morphology of RGO@SiC thin films

Fig. 2a showed the FTIR spectra of SiC before

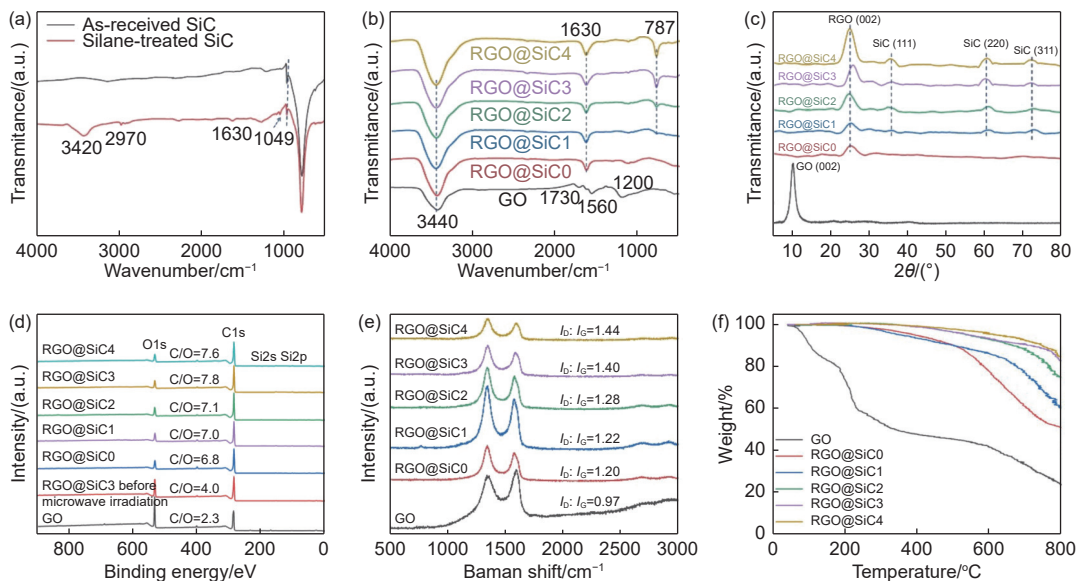


Fig. 2 FTIR spectra of (a) SiC whiskers before and after silanization. (b) FTIR spectra, (c) XRD patterns, (d) XPS spectra, (e) Raman spectra and (f) TGA results of GO and RGO@SiC thin films

and after the silane-treatment, where the strong peak at  $787\text{ cm}^{-1}$  came from C—Si bonding of SiC whiskers. The silane-treated SiC showed extra peaks at  $3420$ ,  $2970$ ,  $1630$  and  $1049\text{ cm}^{-1}$ , corresponding to N—H, C—H,  $\text{NH}_2$  and Si—O—C stretching vibration, respectively, suggesting the grafting of amino-silane molecules on SiC. Electrostatic interaction was enhanced between the amino groups on SiC and the carboxyl groups on GO during the assembly of GO@SiC thin films.

The FTIR spectra of RGO@SiC thin films were shown in Fig. 2b. The characteristic peaks of GO included  $3440\text{ cm}^{-1}$  (—OH),  $1730\text{ cm}^{-1}$  (C=O),  $1560\text{ cm}^{-1}$  (C=C) and  $1200\text{ cm}^{-1}$  (C—O). The peaks of C=O and C—O disappeared upon reduction of GO, while the peak at  $1630\text{ cm}^{-1}$  appeared and attributed to the restore of C=C bonding. With increasing the content of SiC, the peak of C—Si at  $787\text{ cm}^{-1}$  became strong.

Upon reduction, the peak of GO (002) was moved from  $10^\circ$  to  $25^\circ$  of RGO (002) due to the decreased interlayer distance (Fig. 2c). The characteristic peaks of  $\beta$ -SiC at  $35^\circ$ ,  $60^\circ$  and  $71.8^\circ$  appeared with the addition of SiC whiskers, corresponding to the (111), (220) and (311) crystal planes, respectively<sup>[11]</sup>. It's worth noting that the peak intensity of RGO (002) increased with the content of SiC in RGO@SiC thin films, indicating the improved crystallinity and reduction degree of RGO. Table 1 listed the full width at half maximum (FWHM) values and the crystal size along RGO (002) plane calculated according to Scherrer equation. The FWHM of the RGO (002) peaks decreased and the crystal size increased with increasing the SiC content, indicating that the reduction degree of RGO was improved until the SiC content was 20%.

The addition of SiC facilitated the microwave absorption and the RGO/SiC thin film sparked during the solid phase microwave irradiation for less than 1 s, as shown in Fig. 1, while the sparks were not observed for RGO/SiC0 thin film. A large amount of heat was generated during the strong arc discharge in a few seconds<sup>[21-23]</sup>. As a result, GO was quickly reduced and the reduction degree could be tailored by the SiC content.

To confirm the effect of SiC content on the reduction degree of GO, XPS spectra were shown in Fig. 2d. The C/O ratio clearly increased with the SiC content of RGO@SiC thin films and reached the highest value of 7.8 when SiC content was 20%, as listed in Table 1. The RGO/SiC thin films were reduced by a two-step reduction procedure, which was chemical reduction by HI and heat reduction by the solid phase microwave irradiation. Reduction by HI increased the C/O of GO from 2.3 to 4, and the solid phase microwave irradiation increased the C/O ratio from 4 to 7.8 when the SiC content was 20%. Further increase of the SiC content did not promote the reduction degree, which was consistent with the XRD results. Rapid reduction of GO into pristine graphene by 1–2 s of microwaves irradiation has been reported<sup>[23]</sup>, where GO showed strong absorption capacity due to the existence of  $\pi$ - $\pi$  conjugated regions and polyaromatic domains<sup>[24]</sup>. SiC offered extra “heat points” as the dispersed phase in the thin films because its high dielectric constant facilitated the transformation of microwave energy to heat<sup>[25]</sup>.

Raman spectra of RGO@SiC thin films showed D and G peaks of graphene at  $1350$  and  $1580\text{ cm}^{-1}$  (Fig. 2e), corresponding to the defects and  $\text{sp}^2$  carbon, respectively. The intensity ratio of the D and G peaks

**Table 1 FWHM, crystal size, C/O ratio,  $I_D/I_G$ , surface area and average pore size of the RGO@SiC thin films**

Samples	FWHM/(°)	Crystal size/nm	C/O	$I_D : I_G$	Weight loss at 800°C	Surface area/(m <sup>2</sup> /g)	Pore size/nm
GO	—	—	2.3	0.97	76.1%	—	—
RGO/SiC0	3.444	2.371	6.8	1.20	49.0%	24.28	9.24
RGO/SiC1	2.770	2.948	7.0	1.22	39.9%	20.89	13.53
RGO/SiC2	2.726	2.993	7.1	1.28	25.7%	15.06	18.15
RGO/SiC3	2.185	3.742	7.8	1.40	17.4%	12.87	16.85
RGO/SiC4	2.394	3.410	7.6	1.44	15.2%	8.18	28.89

( $I_D/I_G$ ) increased gradually with the SiC content (Table 1), suggesting the microwave absorption promoted the formation of defects in the basal plane of RGO. Thermal stability of the thin films increased with the reduction degree (Fig. 2f). The weight loss of GO was 76.1% due to the decomposition of oxygen-containing functional groups at high temperature. The weight loss was reduced significantly to 15.2% with increasing the SiC content. The RGO@SiC3 and RGO@SiC4 thin films kept stable until 500 °C, suggesting a high end-use temperature.

Morphology of the thin films with different SiC contents was shown in Fig. 3a-f before and after the microwave irradiation. Before the microwave irradiation, a multilayer structure was featured and the thickness of the thin films increased slightly with the SiC content, ranging from 17 to 23  $\mu\text{m}$ . After the microwave irradiation, a porous structure was featured and a significant increase of the film thickness was observed to 100–200  $\mu\text{m}$ . The largest distance between the neighboring graphene layers was observed over 50  $\mu\text{m}$ . The porous structure was due to the thermal shock generated by only 3 s of solid phase microwave irradiation, which removed a large amount of oxygen-containing functional groups and released small molecules suddenly.

The average pore size of the RGO/SiC thin films (Table 1) increased with the SiC content, agreeing well with the SEM observation, although the specific surface area decreased because SiC has a higher density of

3.2  $\text{g}/\text{cm}^3$  than RGO. Porous structure may lead to fragile materials. This was the reason why the two-step reduction of GO@SiC was employed. The chemical reduction by HI will reduce the concentration of oxygen-containing functional groups to a certain extent and the residue groups were reduced to release small molecules, which expanded the layer space and generated pores during the microwave irradiation, so that the flexibility and porosity of the RGO@SiC thin film were balanced.

### 3.2 EMI shielding performance of the RGO/SiC thin films

The electrical conductivities of RGO@SiC films before and after the microwave irradiation were shown in Fig. 4. The electrical conductivity of pure RGO films reached 14.6 S/cm after the reduction by HI, and then decreased to 5.2 S/cm after the microwave irradiation. For all the RGO@SiC thin films, the microwave irradiation decreased the electrical conductivity for over 50%. However, the microwave irradiation increased the degree of reduction as proven by the C/O ratio shown in Fig. 2d. The reason for the decreased electrical conductivity was the significant amount of pores generated by microwave irradiation, which reduced the electrical contacts between neighboring graphene layers. The electrical conductivity of the RGO@SiC films decreased consistently with the content of SiC before the microwave irradiation because the SiC whiskers were nonconductive. However, the electrical conductivities of RGO/SiC1

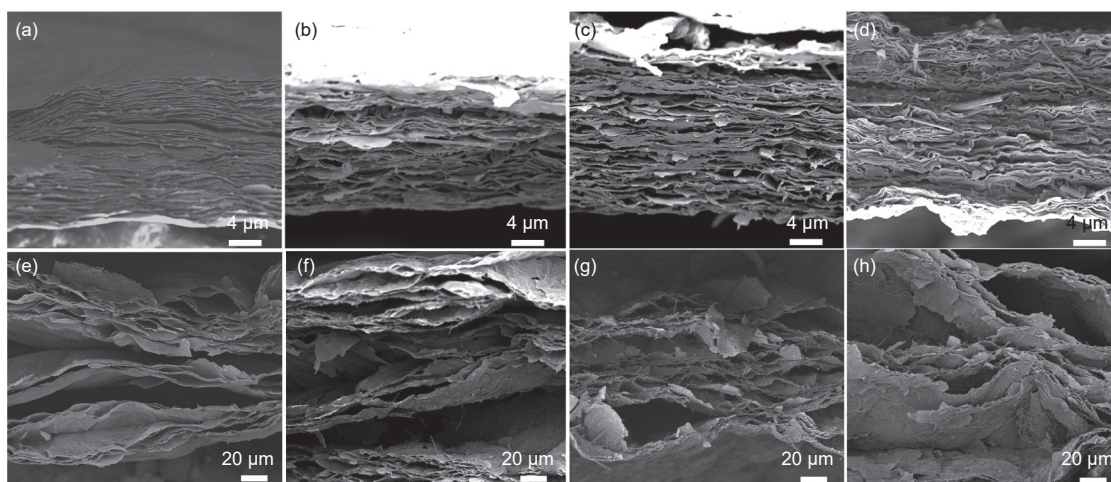


Fig. 3 Cross-section morphology of RGO/SiC0, RGO/SiC1, RGO/SiC2 and RGO/SiC3 thin films (a-d) before and (e-f) after microwave irradiation

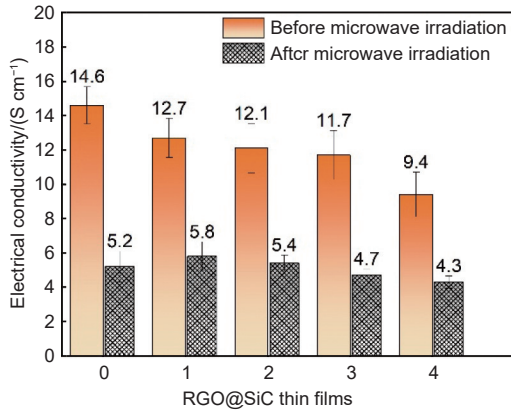


Fig. 4 Electrical conductivities of RGO@SiC thin films before and after microwave irradiation

and RGO/SiC2 were higher a little bit than RGO@SiC0 after the microwave irradiation because 3 effects were combined, namely the reduction degree of RGO, the SiC content and the porosity.

The EMI SE of the thin films was measured in the frequency range of 8.2–12.4 GHz (Fig. 5). The SE<sub>T</sub> increased with the SiC content and reached a maximum value of 29.5 dB for RGO@SiC3 before the microwave irradiation. The improvement was attributed completely to the increase of SE<sub>A</sub>, which was dominated and counted for 27.1 dB, while the SE<sub>R</sub>

was only 2.4 dB. The addition of SiC promoted significantly the absorption of the EM waves by dielectric attenuation, which was consistent with its effect on microwave absorption. Excessive amount of SiC reduced the EMI SE of the RGO@SiC4 thin films probably due to its agglomeration.

The SE<sub>T</sub> of the thin film was further improved for over 20% by the microwave irradiation, as shown in Fig. 6, although the electrical conductivity of the thin films was reduced. The reasons for the significant improvement lied in two aspects, one is the reduction degree of RGO, the other is the generation of the pores in the films. The improvement was again mainly attributed to the SE<sub>A</sub>, noting that the SE<sub>R</sub> values were barely changed before and after the microwave irradiation. The enhanced reduction degree of RGO facilitated the interaction between the EM waves and free charges on each RGO layers in a highly localized scale. In a larger scale, the EM waves underwent an absorption and multi-reflection between neighboring RGO layers and the walls of the pores. The SE<sub>T</sub> values were higher than 30 dB for the porous thin films with SiC. The SE<sub>T</sub> of RGO/SiC3 thin films reached

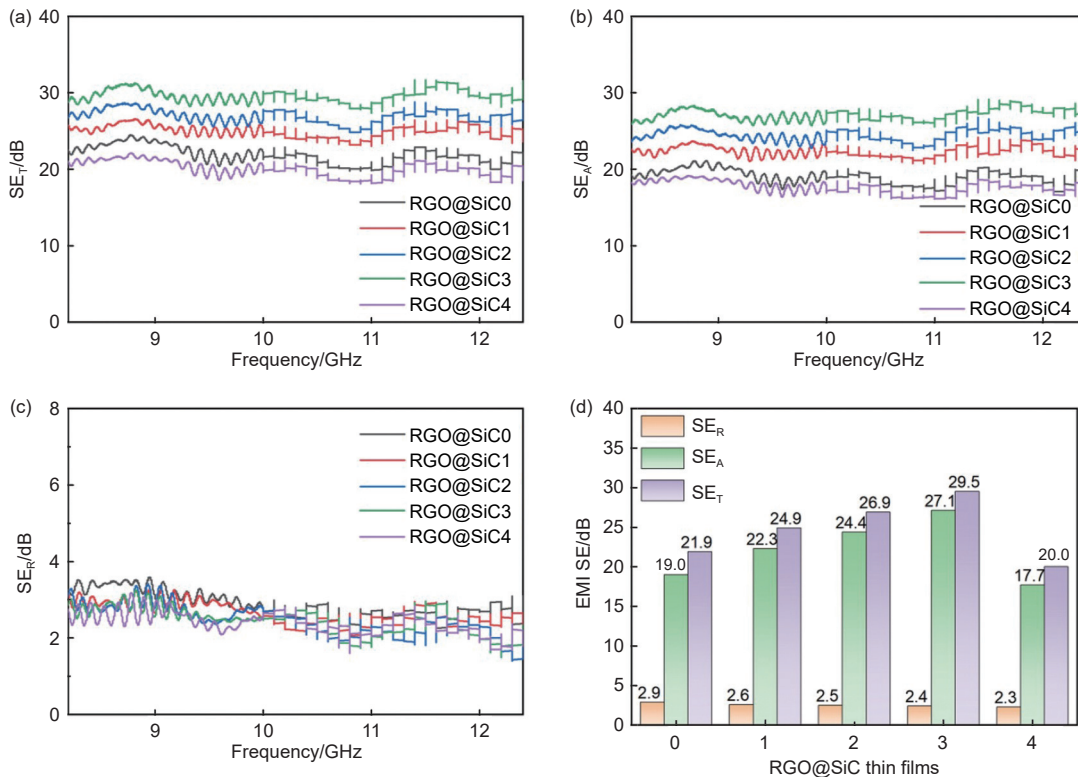


Fig. 5 (a) SE<sub>T</sub>, (b) SE<sub>A</sub>, (c) SE<sub>R</sub> and (d) average SE values of the RGO@SiC thin films before the microwave irradiation

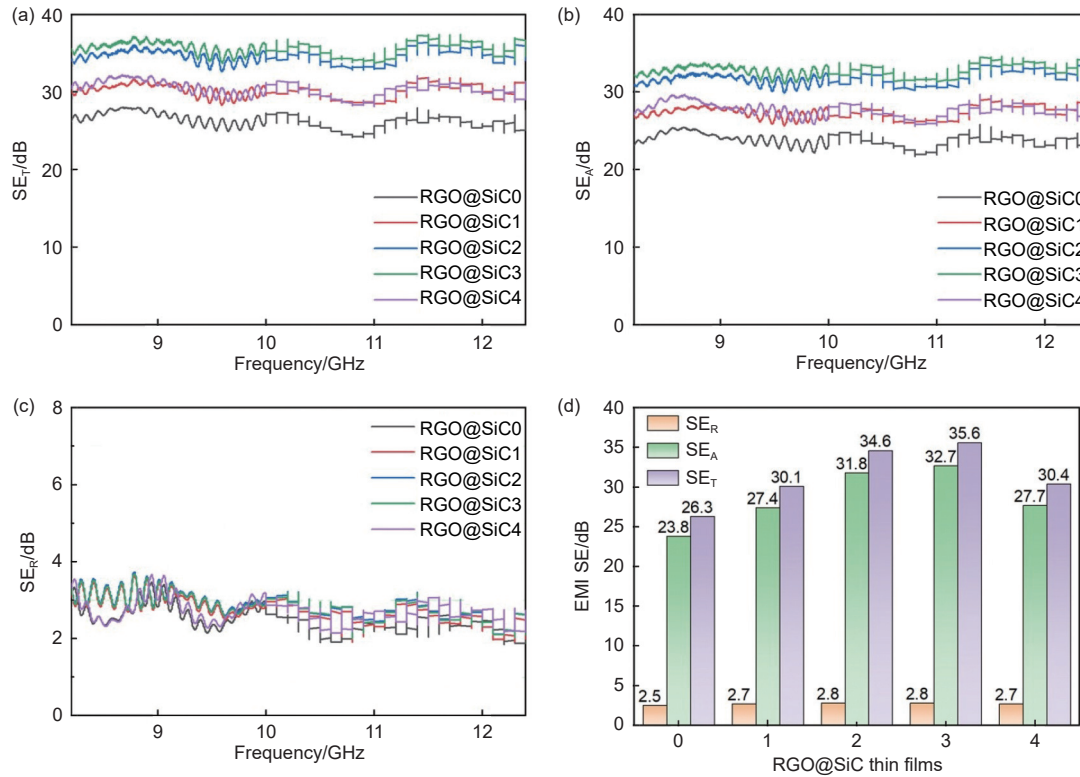


Fig. 6 (a)  $SE_T$ , (b)  $SE_A$ , (c)  $SE_R$  and (d) average SE values of the RGO@SiC thin films after the microwave irradiation

the highest value of 35.6 dB with a  $SE_A$  of 32.7 dB, where the effects of SiC had 3 aspects: (1) Improving the reduction degree of RGO. (2) Promoting the porous structure of the thin films. (3) Introducing dielectric attenuation of EM waves.

### 3.3 Morphology and properties of multilayer composites

Multilayer composites were constructed, as shown in Fig. 7, using MWCNT buckypaper (Fig. 7b) as the reflection layer and WPU with a thickness of around 80  $\mu\text{m}$  (Fig. 1) as the adhesive. Three layers of RGO@SiC thin films were stacked in a sequence (Fig. 7a), where RGO@SiC2, RGO@SiC3, RGO@SiC4 were chosen because they had relatively

low electrical conductivities and high  $SE_T$  values. The thickness of the multilayer composites was slightly over 1.5 mm (Fig. 7c) with a good flexibility (Fig. 1).

To determine the optimal sequence of the 3 RGO@SiC layers, the EMI SE values were compared for all the arrangement without the MWCNT buckypaper (Fig. 8). Apparently, the  $SE_T$  of the composites varied with the arrangement sequence. The highest  $SE_T$  of 66.3 dB and the lowest  $SE_R$  of 2.5 dB were achieved when the three layers of RGO@SiC thin films were arranged in the order of increasing electrical conductivity. When the EM waves were incident from the RGO@SiC layer with lower conductivity, it tended to have a higher  $SE_A$  and lower  $SE_R$ .

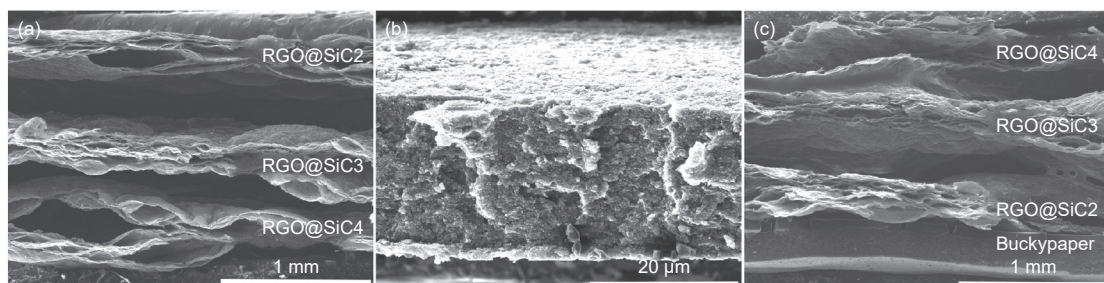


Fig. 7 Morphology of (a) RGO@SiC2/3/4 stacking layers by WPU adhesives, (b) MWCNT buckypaper, and (c) multilayer composites of RGO@SiC4/3/2 and buckypaper as the reflection layers

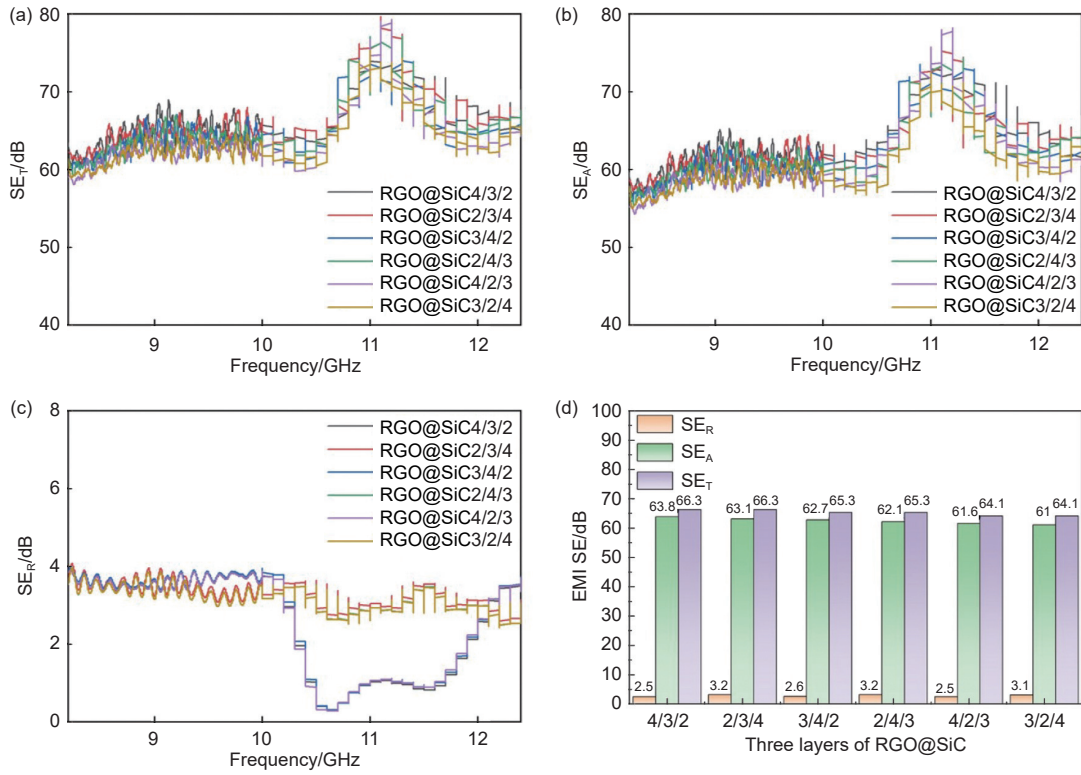


Fig. 8 (a) SE<sub>T</sub>, (b) SE<sub>A</sub>, (c) SE<sub>R</sub> and (d) average SE values for all the stacking sequence of the 3 RGO@SiC layers

The layer with higher conductivity should have higher reflection, which was more suitable for the bottom layer in the arrangement sequence.

With the optimal sequence of RGO@SiC4/3/2 and the MWCNT buckypaper as the reflection layer, their conductivity values were 4.3 S/cm, 4.7 S/cm, 5.4 S/cm and 9.0 S/cm from top to bottom. The SE<sub>T</sub> and SE<sub>R</sub> of the MWCNT buckypaper were 41.0 dB and 3.5 dB (Fig. 9a). Both the electrical conductivity and SE<sub>R</sub> of the MWCNT buckypaper were slightly higher than the RGO@SiC layers, which gave an suitable material selection for the reflection layer to re-

duce the transmission the EM waves and match the impedance between neighboring layers. Thereafter, a four-layer composite was constructed and its EMI SE was compared with a two-layer composites with RGO@SiC3 and buckypaper (Fig. 9b, c). The SE<sub>T</sub> of the 4-layer composite was 32% higher than the 2-layer composite and reached 75.1 dB, meeting the requirement of the high performance EMI shielding material, while the SE<sub>R</sub> value of the four-layer composite was slightly lower than that of the 2-layer composite.

As schematically shown in Fig. 10a, the top layer of RGO@SiC4 had the lowest conductivity and

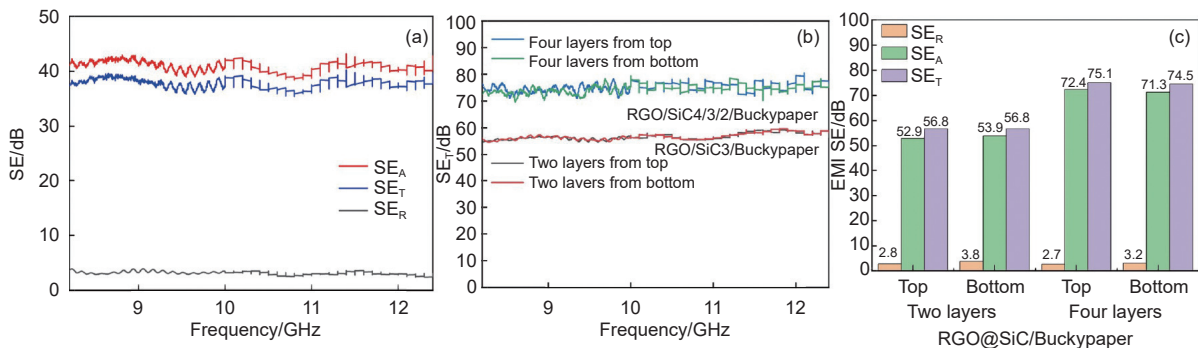


Fig. 9 (a) EMI SE of MWCNT buckypaper. (b) SE<sub>T</sub> and (c) average SE values of the 2-layer and 4-layer composites with incident waves from top and bottom



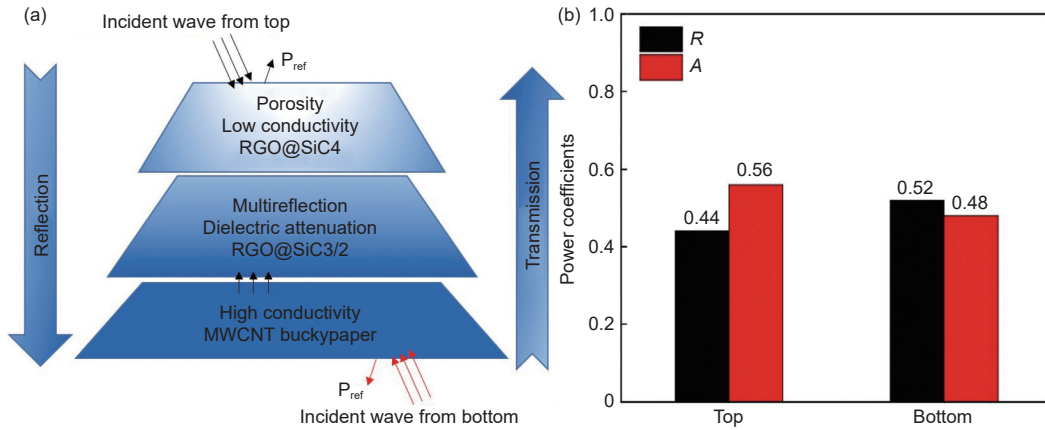


Fig. 10 (a) Mechanism for EMI shielding in the multilayer composites. (b) Average values of  $R$  and  $A$  for the multilayer composites with incident waves from top and bottom

highest average pore size, which gave an impedance matching layer and reduced the reflection<sup>[26]</sup>. In addition, the SiC in the top 3 layers provided not only porosity and dielectric attenuation, but also a large number of heterogeneous interfaces, which improved interfacial polarization. A dense buckypaper layer served to reflect EM waves, benefited from its high electrical conductivity<sup>[27]</sup>. The  $SE_T$  was increased by 13.3% when the MWCNT buckypaper was applied as shown in Fig. 8d and 9c, without much change of  $SE_R$ .

Again, the incident direction affected the portion of  $SE_A$  and  $SE_R$ , while the  $SE_T$  values were barely changed (Fig. 9c). The  $SE_R$  was 2.7 and 3.2 dB when the EM waves were incident from top and bottom layer, respectively. The reflection ( $R$ ) and absorption ( $A$ ) coefficients were calculated according to the Equation (1–3) (Fig. 10b). The transmission coefficient ( $T$ ) can be neglected when the EMI SE was higher than 30 dB<sup>[17]</sup>. The  $A/R$  ratio was higher than 1 when the incident waves were from the top layer (RGO@SiC4), indicating an adsorption-dominated EMI shielding mechanism. Therefore, the top layer should have low conductivity and high porosity for trapping the EM waves. The transmitted EM waves interacted with the center layers (RGO@SiC3/2), which featured intermediate conductivity and high  $SE_A$ . The bottom layer (buckypaper) gave the highest conductivity to enhance the reflection and reduce transmission. Therefore, the interaction between the EM waves and the multilayer composites can be described as absorption/transmission (top) → absorption/multi-reflection (cen-

ter) → reflection (bottom) → re-absorption/multi-reflection (center), which greatly improved the EMI shielding performance (Fig. 10a). A high  $SE_T$  value of over 70 dB has been reported for graphene/WPU composite film with a thickness of 0.9 mm<sup>[28]</sup>, while our multilayer composite films featured the absorption-dominated EMI shielding with a low  $SE_R$  value of 2.7 dB.

## 4 Conclusions

RGO@SiC porous thin films were fabricated by a two-step reduction process, which was chemical reduced by HI and solid phase microwave irradiated for only 3 s. The addition of SiC facilitated the absorption of the microwave, generated sparks and resulted in a high reduction degree of RGO and a large number of pores in the thin films. The electrical conductivity of the RGO@SiC thin films decreased by over 50% while the  $SE_T$  and  $SE_A$  increased by over 20% upon the microwave irradiation. Meanwhile, the addition of 20% SiC whiskers increased the  $SE_T$  by 36.4%. These could be attributed to the multi-reflection, interfacial polarization, dielectric attenuation and impedance matching. Further, the multilayer composites were constructed by stacking the RGO@SiC thin films in a sequence and using the MWCNT buckypaper as the reflection layer. The highest  $SE_T$  reached 75.1 dB with a  $SE_R$  value of 2.7 dB when a thickness was about 1.5 mm. The sequence of the three RGO@SiC layers should be optimally arranged by in-

creasing conductivity from top to bottom, so that a gradient change from transmission to reflection was achieved in addition to the effective absorption of multi-reflected EM waves. We hope the porous RGO@SiC thin films could be a promising material in designing multilayer or sandwich structure for use as EMI absorption packaging or lining materials.

## References

- [ 1 ] Wang Y Y, Zhang F, Li N, et al. Carbon-based aerogels and foams for electromagnetic interference shielding: A review[J]. *Carbon*, 2023, 205: 10-26.
- [ 2 ] Li W, Gao M, Miao Y, et al. Recent progress in increasing the electromagnetic wave absorption of carbon-based materials[J]. *New Carbon Materials*, 2023, 38: 111-129.
- [ 3 ] Zhang F, Li C, Zhang Y, et al. Facile preparation of large-scale expanded graphite/polydimethylsiloxane composites for highly-efficient electromagnetic interference shielding[J]. *Journal of Materials Chemistry A*, 2022, 10: 23145.
- [ 4 ] Xia T, Cao J Y, Bissett M A, et al. Graphenization of graphene oxide films for strongly anisotropic thermal conduction and high electromagnetic interference shielding[J]. *Carbon*, 2023, 215: 118496.
- [ 5 ] Tahalyani J, Akhtar M J, Kar K K. Flexible, stretchable, and thin films based on functionalized carbon nanofiber/graphene nanostructures for electromagnetic interference shielding[J]. *ACS Applied Nano Materials*, 2023, 6: 8178-8191.
- [ 6 ] Wu Y, Wang Z, Liu X, et al. Ultralight graphene foam/conductive polymer composites for exceptional electromagnetic interference shielding[J]. *ACS Applied Materials & Interfaces*, 2017, 9: 9059-9069.
- [ 7 ] Wan Y J, Zhu P L, Yu S H, et al. Graphene paper for exceptional EMI shielding performance using large-sized graphene oxide sheets and doping strategy[J]. *Carbon*, 2017, 122: 74-81.
- [ 8 ] Kumar N, Kuan B K. Single and double-layered tri-band microwave absorbing materials[J]. *Ceramics International*, 2023, 49: 32458-32469.
- [ 9 ] Duan Y, Xiao Z, Yan X, et al. Enhanced electromagnetic microwave absorption property of peapod-like MnO@carbon nanowires[J]. *ACS Applied Materials & Interfaces*, 2018, 10: 40078-40087.
- [ 10 ] Zhao Y, Zhang Y, Yang C, et al. Ultralight and flexible SiC nanoparticle-decorated carbon nanofiber mats for broad-band microwave absorption[J]. *Carbon*, 2021, 171: 474-483.
- [ 11 ] Dong S, Zhang X, Li X, et al. SiC whiskers-reduced graphene oxide composites decorated with MnO nanoparticles for tunable microwave absorption[J]. *Chemical Engineering Journal*, 2020, 392: 123817.
- [ 12 ] Cai Y, Li Y, Huang S, et al. Broadband electromagnetic shielding performance of carbon nanotube-carbon fibre/silicon carbide cross-scale laminated composites[J]. *Ceramics International*, 2022, 48: 26177-26187.
- [ 13 ] Ma L, Hamidinejad M, Liang C, et al. Enhanced electromagnetic wave absorption performance of polymer/SiC-nanowire/MXene ( $\text{Ti}_3\text{C}_2\text{T}_x$ ) composites[J]. *Carbon*, 2021, 179: 408-416.
- [ 14 ] Liang C, Song P, Ma A, et al. Highly oriented three-dimensional structures of  $\text{Fe}_3\text{O}_4$  decorated CNTs/reduced graphene oxide foam/epoxy nanocomposites against electromagnetic pollution[J]. *Composites Science and Technology*, 2019, 181: 107683.
- [ 15 ] Hu B, Guo H, Li J, et al. Dual-encapsulated phase change composites with hierarchical MXene-graphene monoliths in graphene foam for high-efficiency thermal management and electromagnetic interference shielding[J]. *Composites Part B-Engineering*, 2023, 266: 110998.
- [ 16 ] Tang X, Luo J, Hu Z, et al. Ultrathin, flexible, and oxidation-resistant MXene/graphene porous films for efficient electromagnetic interference shielding[J]. *Nano Research*, 2023, 16: 1755-1763.
- [ 17 ] Sheng A, Ren W, Yang Y, et al. Multilayer WPU conductive composites with controllable electro-magnetic gradient for absorption-dominated electromagnetic interference shielding[J]. *Composites Part A: Applied Science and Manufacturing*, 2020, 129: 105692.
- [ 18 ] Yang J, Liao X, Wang G, et al. Heterogeneous silicon rubber composite foam with gradient porous structure for highly absorbed ultra-efficient electromagnetic interference shielding[J]. *Composites Science and Technology*, 2021, 206: 108663.
- [ 19 ] Kim M, Kim S, Seong Y C, et al. Multiwalled carbon nanotube buckypaper/polyacrylonitrile nanofiber composite membranes for electromagnetic interference shielding[J]. *ACS Applied Nano Materials*, 2021, 4(1): 729-738.
- [ 20 ] Hu Y, Li D, Wu L, et al. Carbon nanotube buckypaper and buckypaper/polypropylene composites or high shielding effectiveness and absorption-dominated shielding material[J]. *Composites Science and Technology*, 2019, 181: 107699.
- [ 21 ] Jiang W S, Yang C, Chen G X, et al. Preparation of high-quality graphene using triggered microwave reduction under an air atmosphere[J]. *Journal of Materials Chemistry C*, 2018, 6(7): 1829-1835.
- [ 22 ] Sun Y, Qiu S, Fang Z, et al. Rapid synthesis of oxygen-deficient  $\text{MoO}_3$ -x-rGO composites for synergistic photothermal seawater desalination and photocatalytic sterilization[J]. *ACS Sustainable Chemistry & Engineering*, 2023, 11: 3359-3369.
- [ 23 ] Voiry D, Yang J, Kupferberg J, et al. High-quality graphene via microwave reduction of solution-exfoliated graphene oxide[J]. *Science*, 2016, 353: 1413-1416.
- [ 24 ] Hu H, Zhao Z, Zhou Q, et al. The role of microwave absorption on formation of graphene from graphite oxide[J]. *Carbon*, 2012, 50: 3267-3273.
- [ 25 ] Tamang S, Aravindan S. 3D numerical modelling of microwave heating of SiC susceptor[J]. *Applied Thermal Engineering*, 2019, 162: 114250.
- [ 26 ] Yang W, Yan L, Jiang B, et al. Crumpled nitrogen-doped porous carbon nanosheets derived from petroleum pitch for high-performance and flexible electromagnetic wave absorption [J], *Industrial & Engineering Chemistry Research*, 2022, 61:

2799–2808.

[27] Yang W, Jiang B, Che S, et al. Research progress on carbon-based materials for electromagnetic wave absorption and the related mechanisms[J]. *New Carbon Materials*, 2021, 36: 1016-1033.

[28] Yang W, Bai H, Jiang B, et al. Flexible and densified graphene/waterborne polyurethane composite film with thermal conducting property for high performance electromagnetic interference shielding[J]. *Nano Research*, 2022, 15: 9926-9935.

## 基于还原氧化石墨烯与碳化硅的多孔电磁屏蔽薄膜及其多层结构

李 静\*, 祁奕铨, 赵诗翔, 邱汉迅, 杨俊和, 杨光智\*

(上海理工大学 材料与化学学院, 上海 200093)

**摘 要:** 轻质柔性的电磁屏蔽薄膜材料的开发具有重要的意义。本文报道了一种还原氧化石墨烯与碳化硅 (RGO@SiC) 的多孔状电磁屏蔽薄膜, 其多孔结构由固态微波处理高效获得, 仅 3 s 的处理便可高效还原氧化石墨烯, 同时使薄膜厚度从大约 20  $\mu\text{m}$  增加至 200  $\mu\text{m}$ 。当该薄膜的电磁屏蔽效能达到 35.6 dB 时, 其反射效能仅为 2.8 dB。SiC 晶须在薄膜中的添加有利于电磁波的多次反射、界面极化和介电衰减。进一步, 将 RGO@SiC 多孔薄膜按照透过层到反射层的顺序叠加, 构建多层复合薄膜, 并采用多壁碳纳米管纸作为反射层。当多层结构厚度为 1.5 mm 时, 最高电磁屏蔽效能达到 75.1 dB, 其中反射效能仍保持在 2.7 dB。该多孔状 RGO@SiC 薄膜可用于设计以吸收为主的电磁屏蔽多层封装材料或三明治结构的芯层。

**关键词:** 石墨烯; 薄膜; 碳化硅晶须; 电磁屏蔽

**中图分类号:** TQ127.1<sup>+</sup>1      **文献标识码:** A

**通讯作者:** 李 静, 博士, 教授. E-mail: [lijing6080@usst.edu.cn](mailto:lijing6080@usst.edu.cn);

杨光智, 博士, 教授. E-mail: [yanggzh@usst.edu.cn](mailto:yanggzh@usst.edu.cn)

本文的电子版全文由 Elsevier 出版社在 ScienceDirect 上出版 (<https://www.sciencedirect.com/journal/new-carbon-materials/>)